PNAS RESEARCH ARTICLE | APPLIED PHYSICAL SCIENCES
BIOPHYSICS AND COMPUTATIONAL BIOLOGY OPEN ACCESS

Population genetics in microchannels

Anzhelika Koldaeva[a], Hsieh-Fu Tsai[b], Amy Q. Shen[b], and Simone Pigolotti[a,1]

Edited by David Weitz, Harvard University, Cambridge, MA; received November 15, 2021; accepted February 13, 2022

Spatial constraints, such as rigid barriers, affect the dynamics of cell populations, potentially altering the course of natural evolution. In this paper, we investigate the population genetics of *Escherichia coli* proliferating in microchannels with open ends. Our analysis is based on a population model, in which reproducing cells shift entire lanes of cells toward the open ends of the channel. The model predicts that diversity is lost very rapidly within lanes but at a much slower pace among lanes. As a consequence, two mixed, neutral *E. coli* strains competing in a microchannel must organize into an ordered regular stripe pattern in the course of a few generations. These predictions are in quantitative agreement with our experiments. We also demonstrate that random mutations appearing in the middle of the channel are much more likely to reach fixation than those occurring elsewhere. Our results illustrate fundamental mechanisms of microbial evolution in spatially confined space.

spatial population dynamics | bacterial evolution | microfluidics | individual-based models

Significance

Many microbial populations proliferate in small channels. In such environments, reproducing cells organize in parallel lanes. Reproducing cells shift these lanes, potentially expelling other cells from the channel. In this paper, we combine theory and experiments to understand how these dynamics affects the diversity of a microbial population. We theoretically predict that genetic diversity is quickly lost along lanes of cells. Our experiments confirm that a population of proliferating *Escherichia coli* in a microchannel organizes into lanes of genetically identical cells within a few generations. Our findings elucidate the effect of lane formation on populations evolution, with potential applications ranging from microbial ecology in soil to dynamics of epithelial tissues in higher organisms.

Biological populations can be spatially organized by landscape barriers that constrain individual movement, generating ordered patterns at the population level. For example, populations of rod-shaped bacteria *Escherichia coli* growing on surfaces tend to organize into domains of aligned cells (1, 2). When *E. coli* grows in confined channels, cell alignment is affected by the geometry of the channel boundaries (3, 4). In narrow channels, populations reach a highly ordered structure, with cells organized parallel to each other and to the boundaries (5, 6). In wide channels, such alignment is disrupted at large scales by a buckling instability (7).

Once a cell population densely fills a microchannel, dividing cells push others toward the open ends, potentially leading to expulsion of cells. The timescale at which cells are expelled is typically shorter than their lifetime (an estimate of the latter is, e.g., in ref. 8). Therefore, death events can be usually neglected when focusing on a population inside a microchannel. In genetically diverse populations, we expect such competition to reduce diversity at a pace that depends on the channel dimensions relative to the cell size.

Microfluidic devices constitute ideal experimental systems to study population growth in confined geometries (9). Size and shape of the microchannels in these devices can be tailored to mimic microorganism habitats (10, 11). Nutrients can be delivered to the residing microorganisms inside the microchannels by controlled flows. Such devices are often used to track population dynamics of microorganisms at the single-cell level over several generations (12, 13). A paradigmatic example is the "mother machine"—a microchannel with one open end and small-enough width to accommodate a single lane of cells (8). Microchannels with two open ends have been used to validate a relation between the cell division time distribution and the population growth rate (14), but see (15).

From the theoretical side, competition in confined geometries has been scarcely studied. Common spatial competition models, ranging from Kimura's stepping stone model (16, 17) to generalizations in the theory of evolutionary graphs (18–21), include birth, death, and diffusion events only and do not account for cell to cell mechanical interactions in confined geometries. Single-lane models in which newborn individuals shift their neighbors away have been theoretically studied in the context of cancer progression (22, 23). A microbial population dynamics model incorporating shifting has been investigated with computational approaches (14, 24). In particular, simulations of a model of competing bacterial strains (24) show a formation of lanes along the channel axial direction. Theoretical predictions for geometries hosting multiple lanes and quantitative experimental validations have been lacking.

In this paper, we study the population genetics of bacterial colonies growing in confined geometries. We combine theory, numerical simulations, and experiments on *E. coli* populations growing in rectangular microchannels with two open ends. We introduce our work by first presenting experiments in which two fluorescently marked neutral *E. coli* strains competing in microchannels demix into a stripe pattern. We explain this phenomenon by means of an individual-based population model describing competition between strains inside the channel. This model reveals that the diversity loss within each

Author affiliations: [a]Biological Complexity Unit, Okinawa Institute of Science and Technology and Graduate University, Okinawa 904-0495, Japan; and [b]Micro/Bio/Nanofluidics Unit, Okinawa Institute of Science and Technology and Graduate University, Okinawa 904-0495, Japan

Author contributions: A.K. and S.P. designed the research; A.K. performed numerical simulations and analyzed the data; H.-F.T. and A.Q.S. designed the experiments; H.-F.T. performed experiments; and A.K. and S.P. wrote the paper, with input from H.-F.T. and A.Q.S.

The authors declare no competing interest.

This article is a PNAS Direct Submission.

[1]To whom correspondence may be addressed. Email: simone.pigolotti@oist.jp.

This article contains supporting information online at https://www.pnas.org/lookup/suppl/doi:10.1073/pnas.2120821119/-/DCSupplemental.

Published March 18, 2022.

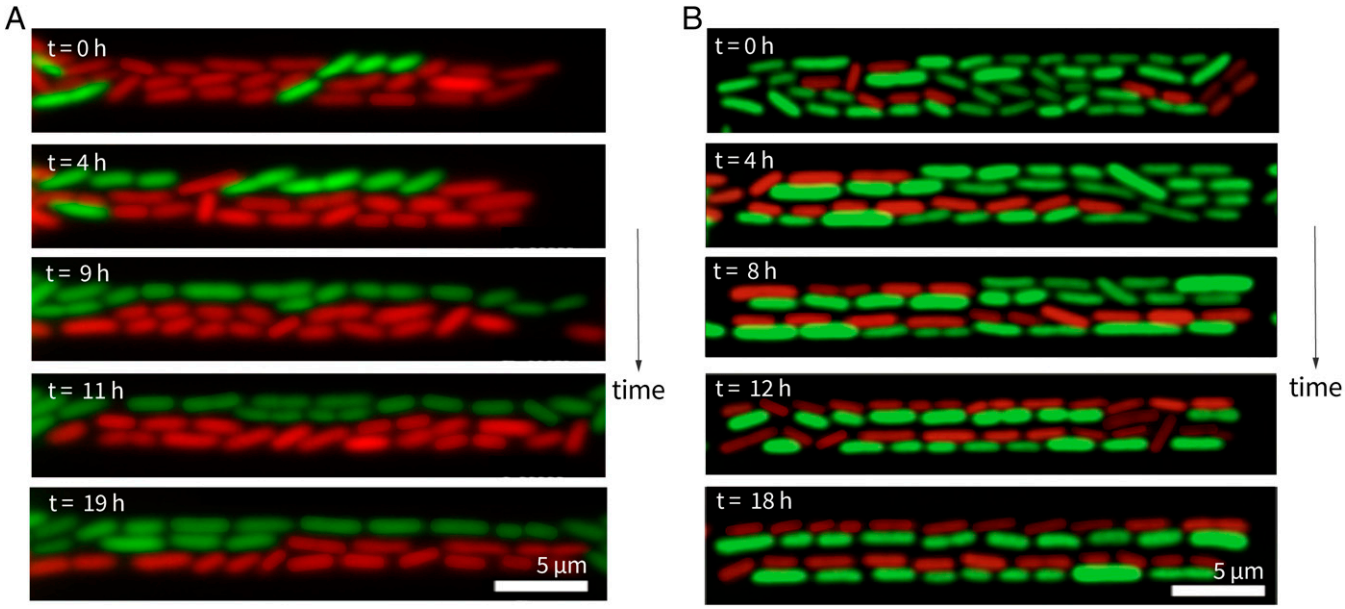

Fig. 1. Competition between two *E. coli* strains (in red and green) in microchannels with two open ends. Two experimental realizations in microchannels of different widths are shown. (*A*) Competing strains form two stripes in a channel of width 2.5 μm harboring three lanes of cells. (*B*) Strains segregate into four stripes in a channel of width 3 μm harboring four lanes of cells. The observed number of stripes fluctuates among different experimental runs (*SI Appendix*, Fig. S1*A*).

lane is much faster than that predicted by traditional spatial population genetics, in quantitative agreement with our experimental observations. We discuss the consequences of our results and their implications for the evolution of cell populations in confined geometries.

Results

Competing Neutral *E. coli* Strains Form Stripe Patterns in Microchannels. As a motivation, we present an experiment that anticipates a main consequence of our theory. We inoculated a mixture of two *E. coli* strains into microchannels (Fig. 1). The two strains are labeled with green fluorescent protein (GFP) and red fluorescent protein and are otherwise neutral (i.e., have the same fitness). Bacteria reproduce in nutrient-rich conditions inside the microchannels and push each other toward the open ends. As a result, cells are continuously expelled, while the number of cells inside the channels remains nearly constant. Our microchannels have a rectangular cross section, are 30-μm long, 1-μm deep, and have variable width from 1 to 3 μm, unless specified otherwise. For comparison, *E. coli* cells are 2.1 ± 0.2 μm in length and 0.65 ± 0.04 μm in width, so that the microchannels host monolayers of cells of width ranging from one to four lanes.

In about 8 h, the two strains organize themselves into regular stripe patterns (Fig. 1 and Movies S1 and S2). The number of stripes and their width depend on the microchannel width and also fluctuate depending on the initial arrangement of inoculated cells. In these experiments, the average cell division time is ∼95 min, meaning that lanes are formed within a few generations. Our focus is on microchannels hosting monolayers of cells, but we also observe stripe formation in deeper (3-μm) microchannels, harboring multiple layers of cells (Movie S3).

Population Model Predicts the Stripe Pattern. We want to understand how the genetic diversity of a microbial population in a microchannel changes with time. We model the microchannel as a lattice of $M \times N$ sites. Each site is always occupied by one cell (Fig. 2*A*). We define clonal populations as groups of cells that originate from a common ancestor in the initial population. The dynamics of the clonal populations permits us to determine the patterns that the population would develop if some of the cells were fluorescently marked or carried a neutral mutation.

The dynamics proceeds as follows. Cells reproduce binarily at a constant rate b. After reproduction, one daughter cell takes the position of its mother. The other occupies one of the adjacent lattice sites and shifts a lane of existing cells toward one open end of the microchannel. As a result, a cell at the open end is expelled from the microchannel. If a reproducing cell is located next to an open end, its daughter can end up outside the microchannel, thereby being immediately expelled.

Our experiments reveal that the probabilities of choosing neighboring sites are not uniform. Specifically, we identify two effects that bias these probabilities. The first effect is related to the mass of the lane of cells to be shifted. We observe that reproduction events that shift shorter lanes of cells are more likely. We quantify this effect via a mass parameter $m \geq 0$. Increasing m biases reproduction in the direction closer to an open end. The second effect is the preference of cells to reproduce within the same lane due to their aligned arrangement and the rod shape of *E. coli*. We introduce an alignment parameter $\alpha > 0$ equal to the relative probability of a reproduction event within a lane over that of an event involving a change of lane. In the limiting case $\alpha = 1$ and $m = 0$, the reproduction probabilities are uniform as in the model numerically studied in ref. 14.

We determine the parameters N, M, b, m, and α from our experiments with a single *E. coli* strain in channels of different width (*Materials and Methods* and *SI Appendix*). We find that N and b are the only parameters that significantly depend on the channel width (Table 1).

We take the number $A(t)$ of clonal populations in the microchannel at time t as our measure of diversity. At the initial time $t = 0$, we have $A(0) = MN$. Diversity decreases with time, as progenies of initial individuals are expelled from the microchannel (Fig. 2*B*). At intermediate times, the surviving strains tend to form stripe patterns that resemble those in Fig. 1 (*SI Appendix*, Fig. S1 shows a more extensive qualitative comparison). The model

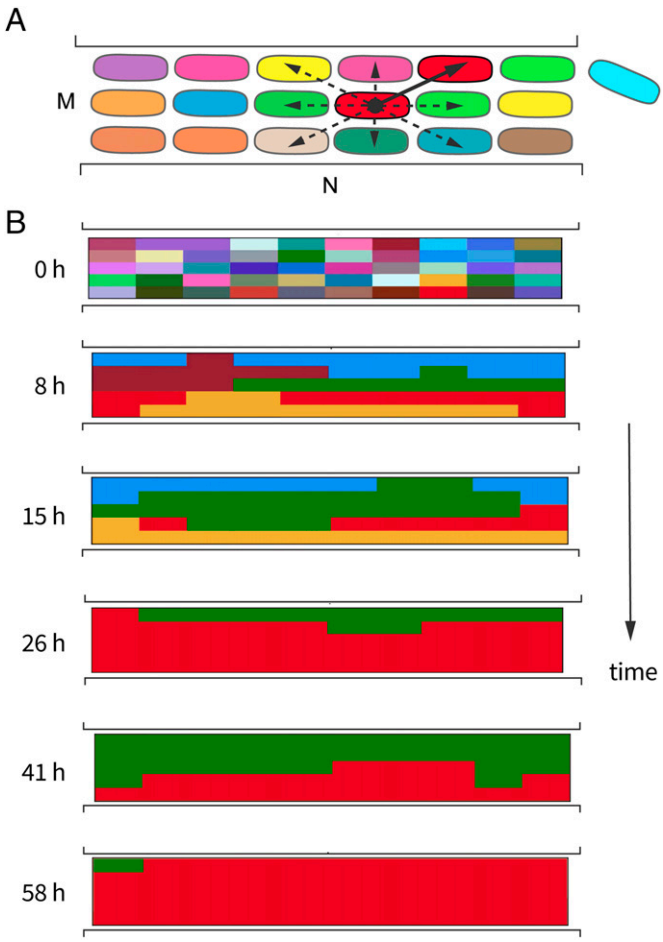

Fig. 2. The population model describes cells proliferating in a microchannel. (*A*) Scheme of the model. The population is made up of M X N individuals. Different colors represent different clonal populations. A randomly chosen cell reproduces to the right (arrow) and shifts all the cells to its right toward the right end of the microchannel. As a result, the cell next to the right end is expelled from the microchannel. Dashed arrows show the other seven possible directions for reproduction. Cells located at the boundaries can reproduce in five possible directions. (*B*) Dynamics of the model. The dynamics progresses until one clonal population takes over the entire population. *SI Appendix*, Fig. S1 shows a more extensive comparison between the patterns observed in experiments and in simulations. Parameters are $M = 5$, $N = 10$, $b = 0.01$ min^{-1}, $m = 0.6$, and $\alpha = 3.2$.

further predicts that competition between stripes should lead to fixation of one of the strains at very long times.

Diversity Loss and Fixation Are Exponentially Fast in Single-Lane Microchannels. We study diversity loss starting from microchannels with a single lane. In this case, we compute the rate of diversity loss by focusing on the interfaces between clonal populations (*Materials and Methods*). We find that the average diversity at time t is equal to

$$\langle A(t)\rangle = (N-1)e^{-\beta t} + 1, \qquad [1]$$

where we define

$$\beta = b\left(1 - \frac{m}{N-1}\right). \qquad [2]$$

Eq. **1** shows that diversity loss in single-lane channels is exponentially fast. This result is in stark contrast with classic spatial population models, such as the voter model, where diversity decays as $t^{-1/2}$ in one dimension (25). The characteristic rate β at which diversity is lost is on the order of the reproduction rate b, apart from a correction term that depends on the mass parameter m.

Table 1. Parameters evaluated from the experimental recordings

Width, μm	M	N	b (1/min)	m	α
1	1	13	0.007	0.6	—
1.5	2	9	0.007	0.6	3.2
2.5	3	9	0.01	0.6	3.2
3	4	9	0.0105	0.6	3.2

At long times, one clonal population eventually takes over the entire microchannel. The time at which this event occurs is called the fixation time. In microchannels with a single lane, the average fixation time is equal to

$$\langle T_{N\to 1}\rangle = \beta^{-1}\sum_{A=2}^{N}\frac{1}{A-1} \approx \beta^{-1}[\log(N-1)+\gamma], \qquad [3]$$

where $\gamma \approx 0.577$ is the Euler–Mascheroni constant, and the approximation is valid for large N (*Materials and Methods*). The logarithmic dependence of the fixation time on the population size N reflects the fact that the number of clonal populations decays exponentially in time (Eq. **1**). The theoretical predictions of Eqs. **1** and **3** are in excellent agreement with our experiments (Fig. 3*A* and Table 2).

First Regime of Diversity Loss: Exponentially Fast Fixation within Each Lane. Our results in the single-lane case suggest that, in microchannels with multiple lanes, competition within each lane should lead to an exponentially fast diversity loss. In contrast, we expect competition among lanes to be less effective at reducing diversity. The alignment of cells favors reproduction events within each lane, further enhancing this difference. Following this idea, we identify two temporal regimes of diversity loss. In the first regime, diversity rapidly decreases from $A = MN$ to $A = M$, primarily due to competition within lanes. The second regime ranges from $A = M$ down to $A = 1$ and is characterized by competition among lanes.

The first regime is characterized by negligible interaction among lanes. It follows from Eq. **1** that the average number of clonal populations at time t is approximated by

$$\langle A(t)\rangle \approx M(N-1)e^{-\beta t} + M. \qquad [4]$$

We test this prediction in experiments with a single *E. coli* strain, where we track descendant of each individual in the initial population (*Materials and Methods*). We find an excellent agreement (Fig. 3*A*). Eq. **4** also implies that the quantity $\log[(\langle A(t)\rangle - M)/(M(N-1))]$ must be a universal linear function of βt (Fig. 3 *A*, *Inset*).

We approximate the average duration $\langle T_{MN\to M}\rangle$ of the first regime as

$$\langle T_{MN\to M}\rangle \approx \beta^{-1}[\log(M(N-1)) + \gamma] \qquad [5]$$

(*SI Appendix*). This approximation and numerical simulations of the model agree well with our experiments (Table 2).

Second Regime of Diversity Loss: Slow Competition among Lanes. In the second temporal regime of diversity loss, competition among lanes becomes relevant. This competition is driven by events in which a cell reproduces in a neighboring lane and its progeny eventually colonizes the entire lane. These events occur at a rate that we estimate to be quite small (*SI Appendix*). Aside

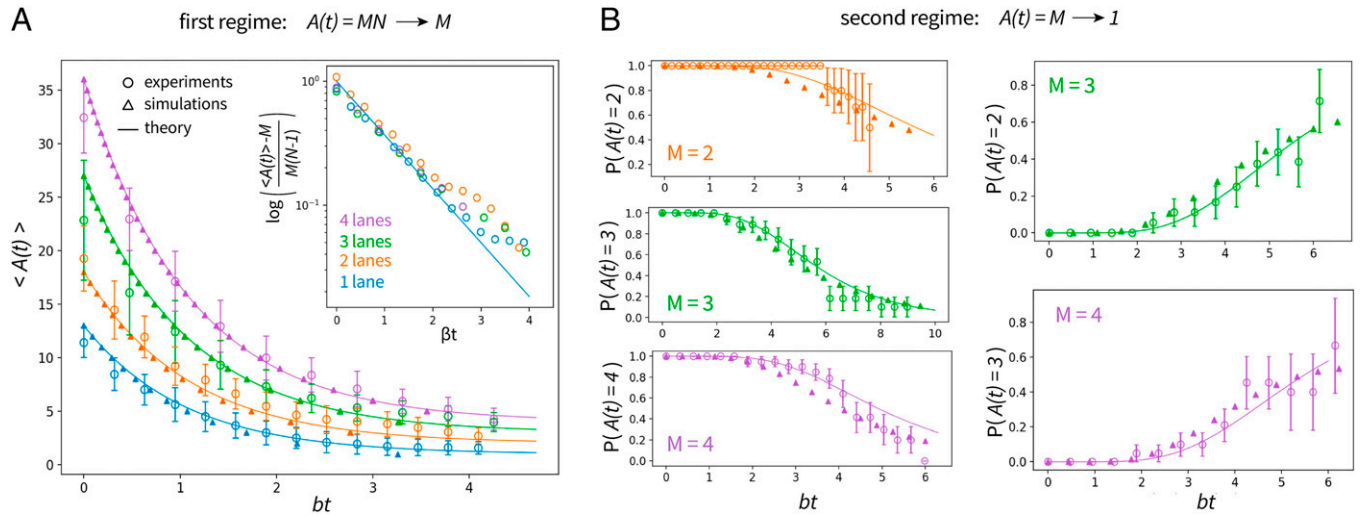

Fig. 3. Two temporal regimes of diversity loss. In all plots, circles with error bars represent the experimental data, triangles represent numerical simulations, and solid curves represent analytical solutions. Model parameters are listed in Table 1. (*A*) The first regime of diversity loss. Theory, simulations, and experiments show that diversity decreases exponentially in time. Time is measured in generations. The solid curves represent the analytical solutions given by Eq. **4**. *A*, *Inset* shows a linear data collapse of the experimental data based on Eq. **4**. (*B*) The second regime of diversity loss. The probability of observing a given number of clonal population as a function of time is measured in generations from the start of the second regime. The experimental data are obtained by retracking our experimental data (*Materials and Methods*). Details on the data analysis and analytical solutions are in *SI Appendix*.

from these events, lanes are typically dominated by a single clonal population (*SI Appendix*).

Following these ideas, we can consider lanes as single units, which invade each other at a certain rate. This process is called the invasion process in the literature (21). We mathematically solve this invasion process and thereby, estimate the probability to observe a given diversity $A(t)$ in the second regime (*SI Appendix*). Our experimental results agree very well with simulations of the model and qualitatively agree with the results from the invasion process (Fig. 3*B*). Our theoretical and numerical results predict that the average fixation time for microchannels with multiple lanes is very long and therefore, inaccessible in our experiments (Table 2).

Exponentially Fast Diversity Loss in the Mother Machine. We extend our theory to quantify the rate of diversity loss in a mother machine. Conceptually, the mother machine is similar to our microchannels with one lane. The main difference is that, in the mother machine, reproductions can occur in only one direction since one end of the microchannel is sealed.

We solve our model with one lane under such conditions (*Materials and Methods*). In this case, we do not consider a mass effect, as the reproduction event can only occur in one direction. We find that, for the mother machine, the diversity loss is still given by Eq. **1** and the average fixation time is given by Eq. **3**, where we set $m = 0$ in both expressions. These results show that the change in boundary conditions does not affect the dynamics of diversity loss.

Cells in the Middle of a Microchannel Possess a Positional Advantage. We expect cells located far from the open ends of the microchannel to benefit from a positional advantage. We quantify this idea by means of the fixation probability $P_{i,j}^{\text{fix}}$, defined as the probability that the clonal population whose initial ancestor has coordinates i, j eventually takes over the microchannel. In the one-lane case and for large N, the fixation probability is approximated by

$$P_i^{\text{fix}} = \phi_{m,N}(i), \qquad [6]$$

where $\phi_{m,N}(i) = \exp[-(i-\mu)^2/(2\sigma^2)]/\sqrt{2\pi\sigma^2}$ is a Gaussian distribution with mean $\mu = (N-1)/2$ and variance $\sigma^2 = (1-m/2)(N-1)/4$ (*SI Appendix*). This means that, at increasing the mass effect, mutants that are likely to take over the population are located in a narrower region at the center of the microchannel (*SI Appendix*, Fig. S3*G*). In particular, the value of the mass parameter that we estimated ($m = 0.6$) leads to a 30% reduction in σ^2, compared with the case $m = 0$.

In microchannels with multiple lanes, we approximate the fixation probabilities by

$$P_{i,j}^{\text{fix}} \approx \begin{cases} \dfrac{2\alpha+6}{M(2\alpha+3)+6}\,\phi_{m,N}(i) & \text{if } j = 1, M \\ \dfrac{2\alpha+3}{M(2\alpha+3)+6}\,\phi_{m,N}(i) & \text{otherwise} \end{cases} \qquad [7]$$

(Fig. 4*A*). The approximation in Eq. **7** is valid in the limit of large N as well. We also require the two regimes of diversity loss to be

Table 2. Mean duration of the first regime $T_{MN\to M}$ and the second regime $T_{M\to 1}$

		$T_{MN\to M}$			$T_{M\to 1}$	
Microchannel width, μm	No. of lanes	Experimental	Theoretical	Numerical	Theoretical	Numerical
1	$M = 1$	3.58 ± 1.4	3.22 ± 1.31	3.26 ± 1.21	–	–
1.5	$M = 2$	4.04 ± 1.19	3.62 ± 1.74	3.95 ± 1.46	5.95 ± 2.61	6.39 ± 3.99
2.5	$M = 3$	4.75 ± 0.79	4.05 ± 1.83	4.28 ± 1.36	14.68 ± 5.56	13.47 ± 8.44
3	$M = 4$	3.86 ± 0.42	4.37 ± 1.89	4.42 ± 1.25	21.25 ± 6.23	22.32 ± 14.04

Time in the experimental data is scaled by the division rate *b* evaluated for each group of data with one, two, three, and four lanes. The associated uncertainties are SDs. Parameters for the theoretical and numerical predictions are summarized in Table 1.

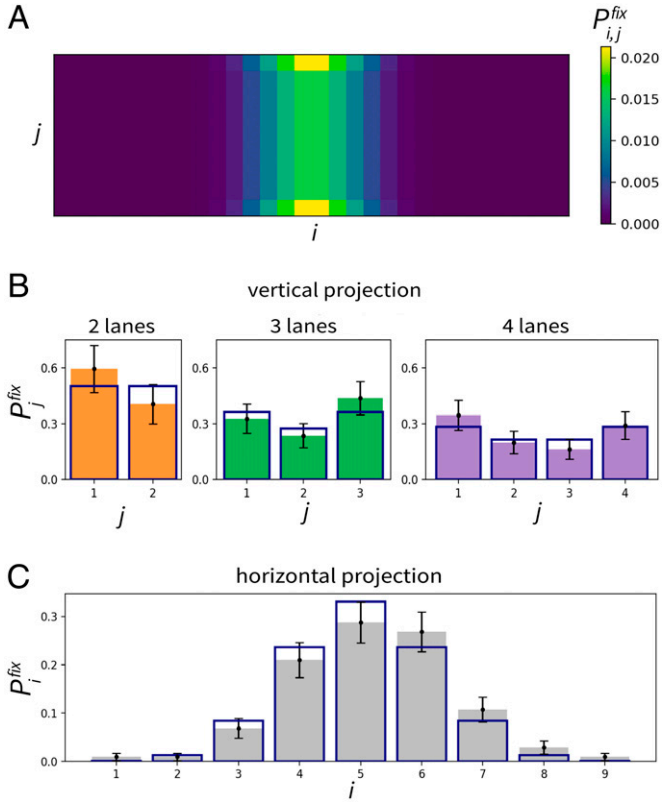

Fig. 4. Fixation probabilities are highest at the center of a microchannel. (*A*) Fixation probabilities predicted by Eq. **7** for $M = 10$, $N = 30$, $m = 0.6$, and $\alpha = 3.2$. (*B*) Fixation probabilities along the vertical (*j*) axis. Color histograms represent empirical probabilities from experiments with associated uncertainties. Dark blue bars represent marginalized fixation probabilities $P_j^{\text{fix}} = \sum_i P_{i,j}^{\text{fix}}$, where $P_{i,j}^{\text{fix}}$ is given in Eq. **7**. The number of cells per lane is $N = 9$ for all three cases. In the experiments where populations do not reach fixation, we use all remaining clonal populations at the end of the experiment (typically, from two to six) to approximate the empirical fixation probabilities. The validity of this approximation is supported by numerical simulations (*SI Appendix*). (*C*) Projections of the fixation probabilities along the horizontal (*i*) axis. The gray histogram represents the empirical fixation probabilities. Dark blue bars represent $P_i^{\text{fix}} = \sum_j P_{i,j}^{\text{fix}}$.

well separated (*SI Appendix*). The fixation probabilities predicted by Eq. **7** are in good agreement with experimental observations (Fig. 4 *B* and *C*).

Discussion

In this paper, we studied the population genetics of microbial populations growing in microchannels with open ends. We base our study on a simple model in which cells are placed in lanes that are shifted by reproduction events. This shifting dynamics, combined with the geometry of the microchannels, causes a fast exponential loss of genetic diversity, rapid fixation within each lane, and slower competition among lanes. Our experiments quantitatively confirm these predictions and reveal that population dynamics generates stripes of clonal populations inside the microchannels. This outcome is in sharp contrast to the case of bacterial populations growing on agar plates, where competing populations organize into sectors whose boundaries perform random walks (26).

Previous population models considered shifting dynamics in a single lane. Allen and Nowak (23) studied a similar model on a one-dimensional ring, concluding that this dynamics does not significantly affect the selection strength. However, a model of epithelial tissues has led to the conclusion that the shift dynamics suppresses selection (22). In this latter model, cells are arranged in a linear array and can be expelled only on one end, in a similar fashion as in the mother machine (8). Therefore, random mutations of the cell next to the opposite end are very likely to reach fixation, whereas fixation probabilities of mutations occurring elsewhere are very small. Our results show that this imbalance in fixation probabilities is a robust consequence of pushing dynamics in channels with multiple lanes and open ends, which does not require a strict geometric constraint imposing all cells to descend from a mother cell.

Our results can be extended to populations growing in wider and deeper channels. In such populations, the ordered lane structure is disrupted at large scales, potentially leading to jamming (27, 28). In fact, crowding is known to affect the outcome of competition among microbial strains even in nonconfined geometries (29, 30). Clarifying the connection between these evidences and our results is an interesting venue for future studies.

Our findings are potentially relevant for microbial ecology in soil. Bacteria in soil are spatially organized into relatively isolated and confined microenvironments (31), where fluid flows supply cells with nutrients (32). Most bacteria colonize micropores with diameter of about three times their body size (33) and in any case, smaller than 6 μm since small pores retain water for longer times. Moreover, bacteria residing in a pore of appropriate size are sheltered against larger predators (34). Although bacteria have very large population sizes, it was estimated that each bacterium in soil interacts with about 120 other individuals on average (35). Taken together, these observations support that the size of our microchannels is comparable with that of typical bacterial microenvironments in soil.

Renewing epithelial tissues in multicellular organisms (36) present a similar spatial organization as the one studied in our work. Two main examples are the epidermis (37) and the intestinal crypt (38). The epidermis consists of multiple compartments of cells that originate from a stem cell layer. These stem cells divide and generate differentiated cells that are shifted toward the top of the compartment and can be eliminated from the tissue once they reach the surface. In the intestine, stem cells divide at the bottom of each crypt, move upward, differentiate, and are removed once they reach the top of the villus. This dynamics permits rapid expulsion of cells that have accumulated deleterious mutations, thereby decreasing the risk of cancer, which would otherwise have high chances to arise in rapidly growing epithelial tissues (39, 40). Similarly, proliferation of intestinal stem cells is thought to be disregulated in carcinogenesis (38). Our findings can potentially be extended to understand evolutionary dynamics of these tissues. In particular, adapting our model to study cancer dynamics would require introducing nonneutral clonal populations, as fitness differences between cell types are important for cancer progression (41, 42). Moreover, cells that carry tumor-promoting mutations can be eliminated by apoptosis or killed by surrounding cells so that more detailed cellular interactions should be considered in this case.

The fact that a constrained geometry has such a drastic impact on population genetics should be taken into account when designing experimental evolutionary studies. Our results open possibilities for constraining evolution by shaping the geometry of a microchannel hosting a microbial population.

Materials and Methods

Bacteria Strains and Maintenance. MG1655, a derivative of the *E. coli* K-12 wild-type strain, was used in this study. We transformed a plasmid in MG1655 to constitutively express GFP (pUA66 PrpsL-GFP Kan^R) (43). For the red fluorescent

strain, the pUA66 plasmid with mCherry open reading frame replacing that of GFP was customly constructed (VectorBuilder). We cultured the MG1655 hosting pUA66 plasmids in Luria–Bertani (LB) broth (Lennox) supplemented with 50 μg mL^{-1} kanamycin. A detailed description of bacteria culture and plasmid engineering is provided in *SI Appendix*.

Microfluidic Chip Design and Microfabrication Protocols. The poly(dimethylsiloxane) (PDMS) device (on top of the cover glass) consisted of the top flow channels for nutrients delivery and bacteria removal and the bottom growth channels for bacteria growth, removal, and monitoring (*SI Appendix*, Fig. S2*A*). In order to perfuse fresh nutrients and create flow to remove bacteria, 20 growth channels of different width were intersected with 16 flow channels (Length $\times$ Width $\times$ Height [L $\times$ W $\times$ H] = 4500 $\times$ 50 $\times$ 15 μm). Growth channels (L $\times$ H = 30 $\times$ 1 μm) with varying widths (1, 1.5, 2.5, and 3 μm) and interspacing of 10 μm were designed such that bacteria could be expelled from both ends, in contrast to the single-end design of the mother machine (8, 44). The flow channels were joined by flow-equalizing tree-like channels and flow resistors on both ends (45) and connected to an inlet and an outlet.

A silicon mold with the microstructures designed as above was fabricated by multistep lithography with negative photoresist and maskless direct writing. PDMS microfluidic devices (Sylgard 184; Dow Corning) were fabricated by standard soft lithography (46). The PDMS slab was first cut and punched with an inlet and outlet using a puncher; then, it was bonded to a high-precision cover glass using plasma activation. A 2-mm-thick acrylic frame was cut with a CO_2 laser cutter and affixed on top of the PDMS as a reservoir for bacteria seeding, completing the fabrication of the integrated microdevice. Detailed information of design and microfabrication is provided in *SI Appendix*.

Bacterial Lineage Tracking and Time-Lapse Microscopy. Log-phase MG1655 *E. coli* harboring plasmids for fluorescent proteins was grown at 37° C with vigorous shaking in LB broth supplemented with antibiotic kanamycin until the optical density at 600 nm reached 0.2. The bacteria suspension was concentrated 20 times by centrifugation before being injected into the PDMS microdevice, which was pretreated with a passivation solution to reduce bacterial binding to the microdevice surfaces. The PDMS microdevice was mounted in a microscope on-stage incubator preequilibrated at 37° C on an inverted motorized epifluorescence microscope. The bacteria were allowed to enter the growth channels under static conditions for 2 h before the M9 media were infused using a syringe pump first at a flow rate of 1.6 μL min^{-1}, doubling every 2 h until it reached 16 μL min^{-1}.

The fluorescence images were taken with either a 100$\times$ oil immersion objective or a 60 $\times$ oil immersion objective with 1.5$\times$ intermediate magnification at an interval of $\Delta t = 3$ min using a high-sensitivity camera (Prime95B; Photometrics) with GFP or mCherry filter cubes. More details are provided in *SI Appendix*.

Image Analysis and Data Processing. We processed the time-lapse recordings of our experiments using ImageJ software (47). We used the MicrobeJ plugin to detect bacteria in each frame (48) and a custom Python program to track all the bacteria in time. The tracking algorithm is based on construction and comparison of local structures for each cell (*SI Appendix*, Fig. S3*A*). We then reconstructed spatial lineage trees for each cell in the channel (*SI Appendix*, Fig. S3*B*).

In experiments with multiple lanes, microscopy focus drift issues for long-term live cell imaging experiments caused occasional quality loss in the recordings for a few frames. We cropped the recordings when such issues occurred. The durations of our recordings after this operation are 13.4 ± 4.7h, 9.7 ± 2h, and 7.93 ± 1.5h, corresponding to 5.64 ± 2.02, 5.84 ± 1.35, and 4.76 ± 0.95 generations for the experiments with two, three, and four lanes, respectively.

To explore the second regime, we perform a retracking of the experimental data (*SI Appendix*). In the retracking, we consider an initial condition, in which each lane is occupied by a single clonal population. Retracking is justified by the observation that, during the time at which $A(t) = M$ in our original tracking, at least 70% of each lane is occupied by a single clonal population (*SI Appendix*).

Reproduction Rates and Model Parameters. We assign to each cell its coordinates (i, j), with $1 \leq i \leq N$ and $1 \leq j \leq M$. In the following, we refer to the coordinate i as the "horizontal" or "axial" coordinate. We define the reproduction probability $k_{(i'j')(i,j)}$ as the probability that the daughter of a cell at position i, j is placed at position i', j'.

We start from the case with one lane, $M = 1$. In this case, the probabilities $p(i) = k_{i-1,i}$ and $q(i) = k_{i+1,i}$ that a cell at position i reproduces to the left and right, respectively, are expressed by

$$p(i) = -\frac{im}{N-1} + \frac{m(N+1)+N-1}{2(N-1)}, \quad q(i) = 1-p(i), \qquad [8]$$

where m is the mass parameter. These probabilities depend linearly on i, as observed in experiments (Fig. 5*D*).

In the case $M > 1$, we determine the reproduction probabilities by imposing two constraints. First, the probabilities to divide to the left $k_{(i-1,j)(i,j)}$ and to the right $k_{(i+1,j)(i,j)}$ satisfy the condition $k_{(i-1,j')(i,j)}/k_{(i+1,j')(i,j)} = p(i)/q(i)$

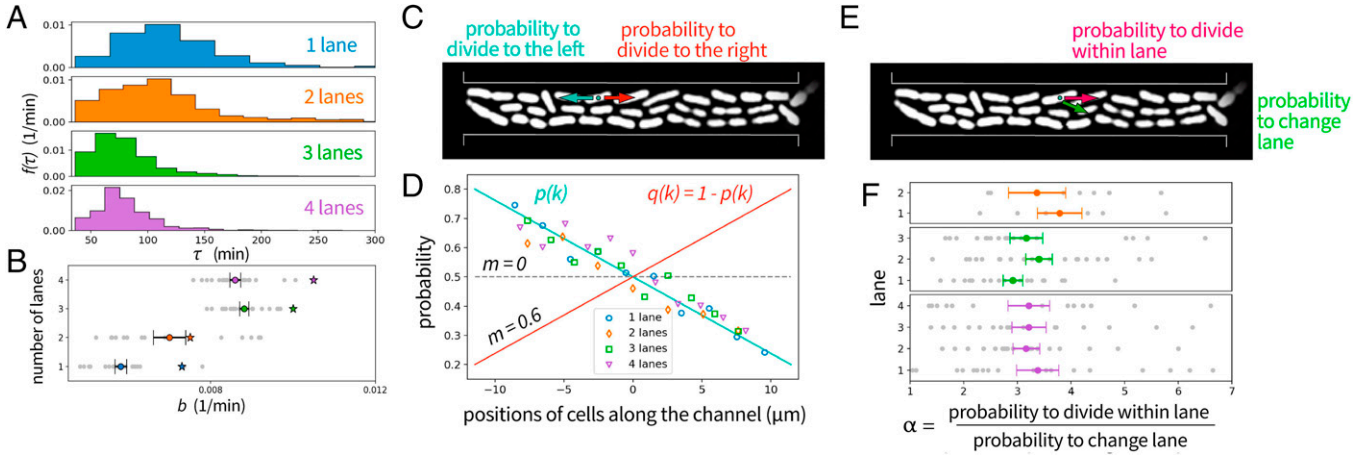

Fig. 5. Estimation of the model parameters from experimental observations. (*A*) Empirical distributions of division times. (*B*) Growth rates evaluated from the experimental data. The error bars represent the mean values and the SEs of the population growth rates obtained as $\ln(\langle 2 \rangle)/\langle \tau \rangle$, where $\langle \tau \rangle$ is the cell division time averaged over the population in a single experimental run. The stars mark the reproduction rates b evaluated by solving the Euler–Lotka equation $2\langle \exp(-b\tau) \rangle = 1$ (*SI Appendix*). (*C*) Scheme of the two possible directions of division. We interpret an asymmetry between frequencies of reproductions in these two directions as a mass effect. (*D*) Mass effect in the experimental data. The scattered points represent the average frequencies of leftward divisions as a function of the cell position in the experimental data. We fit the data with the linear function given in Eq. **8** using the least squares method, resulting in $m = 0.6$ for all channel widths. (*E*) Division within the same lane and to a neighbor lane. The alignment parameter α is defined as the ratio between the probability of a cell division within a lane and that of a cell division involving a change of lane. (*F*) Average value and the SE of α estimated from the experimental data. We find that α does not significantly vary across experiments and lanes. The average value over all experiments is $\alpha = 3.2$. The averages are calculated over 17 microchannels with two lanes, 21 microchannels with three lanes, and 20 microchannels with four lanes.

for $j' = (j-1, j, j+1)$. Second, the ratio between the probability of a cell division within a lane and that of a cell division involving a change of lane must be equal to α: $k_{(i'j)(i,j)}/k_{(i'j')(i,j)} = \alpha$ with $i' = (i-1, i+1)$ and $j' = (j-1, j+1)$.

The reproduction probabilities for cells in the bulk of the population ($1 < j < M$) satisfying these constraints are expressed by

$$\begin{aligned}
k_{(i-1,j)(i,j)} &= \alpha\frac{-2mi + m(N+1) + N - 1}{2(N-1)(\alpha+3)},\\
k_{(i+1,j)(i,j)} &= \frac{2\alpha}{2(\alpha+3)} - k_{(i-1,j)(i,j)},\\
k_{(i-1,j-1)(i,j)} &= k_{(i-1,j+1)(i,j)} = \frac{k_{(i-1,j)(i,j)}}{\alpha},\\
k_{(i+1,j-1)(i,j)} &= k_{(i+1,j+1)(i,j)} = \frac{k_{(i+1,j)(i,j)}}{\alpha},\\
k_{(i,j-1)(i,j)} &= k_{(i,j+1)(i,j)} = \frac{1}{2(\alpha+3)}.
\end{aligned} \qquad [9]$$

If $i' = i$, the lane of cells j' is shifted either to the left or the right with probabilities given by Eq. **8**.

We impose the same constraints for cells next to the top boundary of the microchannel ($j = 1$), obtaining

$$\begin{aligned}
k_{(i-1,1)(i,1)} &= \alpha\frac{-2mi + m(N+1) + N - 1}{(N-1)(2\alpha+3)},\\
k_{(i+1,1)(i,1)} &= \frac{2\alpha}{2\alpha+3} - k_{(i-1,1)(i,1)},\\
k_{(i-1,2)(i,1)} &= \frac{k_{(i-1,1)(i,1)}}{\alpha},\\
k_{(i+1,2)(i,1)} &= \frac{k_{(i+1,1)(i,1)}}{\alpha},\\
k_{(i,2)(i,1)} &= \frac{1}{2\alpha+3}.
\end{aligned} \qquad [10]$$

The reproduction probabilities for cells next to the bottom boundary ($j = M$) can be similarly expressed. In all cases, if the i coordinate of the daughter is equal to zero or $N+1$, she is immediately expelled from the microchannel.

The model parameters evaluated from experiments are summarized in Table 1. For each microchannel width, we estimated M and N as the average number of lanes and the average number of cells per lane in our experiments, respectively. *SI Appendix* has details. The estimation of parameters b, m, and α is detailed in Fig. 5.

Dynamics of Interfaces. We consider the case $M = 1$ and assign to each cell at position i at time t the position $f_i(t)$ of its ancestor at time $t = 0$. The quantity $f_i(t)$ changes every time the cell at position i is replaced by another one having a different initial ancestor. Two neighboring cells having the same value of $f_i(t)$ are conspecific (i.e., they belong to the same clonal population). We assign interfaces to neighboring cells that are not conspecific. We encode these interfaces into a vector $\vec{\sigma}(t) = (\sigma_1(t), \sigma_2(t), \ldots, \sigma_{N-1}(t))$, whose components are defined by

$$\sigma_i(t) = \begin{cases} 0 & \text{if } f_i(t) = f_{i+1}(t),\\ 1 & \text{if } f_i(t) \neq f_{i+1}(t). \end{cases} \qquad [11]$$

The initial condition is $\vec{\sigma}(0) = (1, 1, \ldots, 1)$. The vector of interfaces evolves until it reaches the absorbing state $(0, 0, \ldots, 0)$ that corresponds to fixation of one clonal population. Each cell division creates a pair of conspecific cells and shifts all cells by one position, either to their right or to their left. This event implies that one interface $\{\sigma_i\}_{i=1,\ldots,N-1}$ is set to zero, and all interfaces on one side of it are shifted by one position, depending on the direction of the cell division. As a consequence, an interface located at the open end may be removed from the vector (Fig. 6).

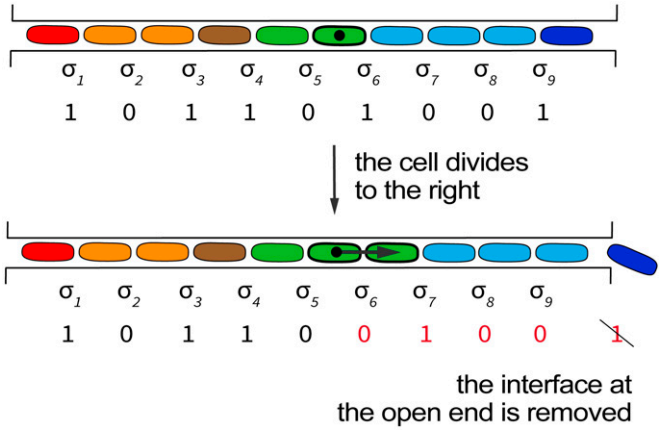

Fig. 6. Dynamics of interfaces. Different colors correspond to different clonal populations. Interfaces $\sigma_1, \sigma_2 \ldots \sigma_{N-1}$ are associated with adjacent cells. An interface σ_i is equal to one if the two associated cells belong to different clonal populations and zero otherwise. As a consequence of cell division, an interface of value zero is created at $i = 6$, and a portion of the vector of interface is shifted (in red). As an outcome, one interface is expelled.

To describe the interface dynamics, we introduce inverse shift operators that take into account the presence or absence of an interface at the open end:

$$\begin{aligned}
\hat{b}_r^i\vec{\sigma} &= (\sigma_1, \sigma_2, \ldots, \sigma_{i-1}, \sigma_{i+1}, \ldots, \sigma_{N-1}, 0),\\
\hat{b}_l^i\vec{\sigma} &= (0, \sigma_1, \sigma_2, \ldots, \sigma_{i-1}, \sigma_{i+1}, \ldots, \sigma_{N-1}),\\
\hat{c}_r^i\vec{\sigma} &= (\sigma_1, \sigma_2, \ldots, \sigma_{i-1}, \sigma_{i+1}, \ldots, \sigma_{N-1}, 1),\\
\hat{c}_l^i\vec{\sigma} &= (1, \sigma_1, \sigma_2, \ldots, \sigma_{i-1}, \sigma_{i+1}, \ldots, \sigma_{N-1}).
\end{aligned} \qquad [12]$$

A state $\hat{b}_r^i\vec{\sigma}$ or $\hat{c}_r^i\vec{\sigma}$ evolves to a state $\vec{\sigma}$ if the ith cell divides to the right. Similarly, a state $\hat{b}_l^i\vec{\sigma}$ or $\hat{c}_l^i\vec{\sigma}$ evolves to a state $\vec{\sigma}$ if the $(i+1)$ th cell divides to the left. The master equation for the interface distribution is

$$\begin{aligned}
\frac{dP_{\vec{\sigma}}}{dt} = &-b\sum_{i=1}^{N-1}[q(i) + p(i+1)]P_{\vec{\sigma}}(t) +\\
&+ b\sum_{i=1}^{N-1}\delta_{\sigma_i,0}[q(i)(P_{\hat{b}_r^i\vec{\sigma}} + P_{\hat{c}_r^i\vec{\sigma}}) + p(i+1)(P_{\hat{b}_l^i\vec{\sigma}} + P_{\hat{c}_l^i\vec{\sigma}})],
\end{aligned} \qquad [13]$$

where $p(i)$ and $q(i)$ are defined in Eq. **8** and the Kronecker delta takes care of the fact that a reproduction event necessarily creates an interface of value equal to zero. The solution of Eq. **13** reads

$$P_{\vec{\sigma}} = \prod_{i=1}^{N-1}\left[\sigma_i e^{-\beta t} + (1-\sigma_i)(1-e^{-\beta t})\right], \qquad [14]$$

where β is defined in Eq. **2**. The solution given in Eq. **14** can be verified by direct substitution into Eq. **13**. Eq. **14** shows that the interfaces $\{\sigma_i(t)\}_{i=1,\ldots,N-1}$ are independent, identically distributed random variables with $P(\sigma_i(t) = 1) = e^{-\beta t}$ for all i. The diversity is related to the number of interfaces by

$$A(t) = \sum_{i=1}^{N-1}\sigma_i(t) + 1. \qquad [15]$$

Computing the average of $A(t)$ using Eq. **14** leads to Eq. **1**.

Fixation Time in the Model with One Lane. We calculate the fixation time for the model with $M = 1$, employing the interface formalism. Removing one interface amounts to removing one clonal population. We denote by $T_{A\to A-1}$ the time it takes to remove the Ath clonal population. The fact that the interfaces $\sigma_i(t)$ are independent, identically distributed random variables implies that the time intervals $T_{A\to A-1}$ are exponentially distributed with mean $\langle T_{A\to A-1}\rangle = 1/[\beta(A-1)]$. This observation directly implies Eq. **3**.

Fixation Time in the Mother Machine. We apply the interface formalism to a model of the mother machine. Without loss of generality, we assume that the open end is the right one. Therefore, the vector of interfaces evolves according to a master equation including only right inverse shift operators:

$$\frac{dP_{\vec{\sigma}}}{dt} = -b(N-1)P_{\vec{\sigma}}(t) + b\sum_{i=1}^{N-1}\delta_{\sigma_i,0}(P_{\hat{b}_r^i\vec{\sigma}} + P_{\hat{c}_r^i\vec{\sigma}}) \qquad \textbf{[16]}$$

(Eqs. **12** and **13**). The solution to this master equation also factorizes

$$P_{\vec{\sigma}} = \prod_{i=1}^{N-1}[\sigma_i e^{-bt} + (1-\sigma_i)(1-e^{-bt})]. \qquad \textbf{[17]}$$

It follows that Eq. **3** with $\beta = b$ holds for the mother machine as well.

Data Availability. All study data are included in the article and/or supporting information.

ACKNOWLEDGMENTS. We acknowledge the support of the Okinawa Institute of Science and Technology Graduate University (OIST) with subsidy funding from the Cabinet Office, Government of Japan. We are grateful for the help and support provided by the Scientific Computing and Data Analysis section of the Research Support Division at OIST. We thank colleagues from the Micro/Bio/Nanofluidics Unit at OIST: Daniel Carlson for assistance in numerical simulation and Riccardo Funari for fruitful discussion; Professor Paola Laurino from OIST for gifting the MG1655 strain and Dr. Pamela Silver from Harvard University for gifting the pUA66 PrpsL-GFP plasmid; and Deepak Bhat, Massimo Cencini, Kirill Korolev, and Robert Ross for feedback on a preliminary version of the manuscript.

1. Z. You, D. J. Pearce, A. Sengupta, L. Giomi, Geometry and mechanics of microdomains in growing bacterial colonies. *Phys. Rev. X* **8**, 031065 (2018).
2. D. Dell'Arciprete *et al.*, A growing bacterial colony in two dimensions as an active nematic. *Nat. Commun.* **9**, 1–9 (2018).
3. H. Cho *et al.*, Self-organization in high-density bacterial colonies: Efficient crowd control. *PLoS Biol.* **5**, e302 (2007).
4. B. R. Karamched *et al.*, Moran model of spatial alignment in microbial colonies. *Physica D* **395**, 1–6 (2019).
5. J. Sheats, B. Sclavi, M. Cosentino Lagomarsino, P. Cicuta, K. D. Dorfman, Role of growth rate on the orientational alignment of *Escherichia coli* in a slit. *R. Soc. Open Sci.* **4**, 170463 (2017).
6. D. Volfson, S. Cookson, J. Hasty, L. S. Tsimring, Biomechanical ordering of dense cell populations. *Proc. Natl. Acad. Sci. U.S.A.* **105**, 15346–15351 (2008).
7. D. Boyer *et al.*, Buckling instability in ordered bacterial colonies. *Phys. Biol.* **8**, 026008 (2011).
8. P. Wang *et al.*, Robust growth of *Escherichia coli*. *Curr. Biol.* **20**, 1099–1103 (2010).
9. E. Levien, J. Min, J. Kondev, A. Amir, Non-genetic variability in microbial populations: survival strategy or nuisance? *Rep. Prog. Phys.* **84**, 116601 (2021).
10. R. Rusconi, M. Garren, R. Stocker, Microfluidics expanding the frontiers of microbial ecology. *Annu. Rev. Biophys.* **43**, 65–91 (2014).
11. K. Kwapiszewska, R. Kwapiszewski, Z. Brzózka, Microfluidic devices as tools for mimicking in vivo environment. *New J. Chem.* **35**, 979–990 (2011).
12. J. Männik, R. Driessen, P. Galajda, J. E. Keymer, C. Dekker, Bacterial growth and motility in sub-micron constrictions. *Proc. Natl. Acad. Sci. U.S.A.* **106**, 14861–14866 (2009).
13. W. Mather, O. Mondragón-Palomino, T. Danino, J. Hasty, L. S. Tsimring, Streaming instability in growing cell populations. *Phys. Rev. Lett.* **104**, 208101 (2010).
14. M. Hashimoto *et al.*, Noise-driven growth rate gain in clonal cellular populations. *Proc. Natl. Acad. Sci. U.S.A.* **113**, 3251–3256 (2016).
15. J. Lin, A. Amir, The effects of stochasticity at the single-cell level and cell size control on the population growth. *Cell Syst.* **5**, 358–367 (2017).
16. M. Kimura, G. H. Weiss, The stepping stone model of population structure and the decrease of genetic correlation with distance. *Genetics* **49**, 561–576 (1964).
17. K. S. Korolev, M. Avlund, O. Hallatschek, D. R. Nelson, Genetic demixing and evolution in linear stepping stone models. *Rev. Mod. Phys.* **82**, 1691–1718 (2010).
18. E. Lieberman, C. Hauert, M. A. Nowak, Evolutionary dynamics on graphs. *Nature* **433**, 312–316 (2005).
19. G. Bradburd, P. L. Ralph, Spatial population genetics: It's about time. *Annu. Rev. Ecol. Evol. Syst.* **50**, 427–449 (2019).
20. M. A. Nowak, C. E. Tarnita, T. Antal, Evolutionary dynamics in structured populations. *Philos. Trans. R. Soc. Lond. B Biol. Sci.* **365**, 19–30 (2010).
21. V. Sood, T. Antal, S. Redner, Voter models on heterogeneous networks. *Phys. Rev. E Stat. Nonlin. Soft Matter Phys.* **77**, 041121 (2008).
22. M. A. Nowak, F. Michor, Y. Iwasa, The linear process of somatic evolution. *Proc. Natl. Acad. Sci. U.S.A.* **100**, 14966–14969 (2003).
23. B. Allen, M. A. Nowak, Evolutionary shift dynamics on a cycle. *J. Theor. Biol.* **311**, 28–39 (2012).
24. T. Shimaya, K. A. Takeuchi, Lane formation and critical coarsening in a model of bacterial competition. *Phys. Rev. E* **99**, 042403 (2019).
25. M. Bramson, D. Griffeath, Asymptotics for interacting particle systems on Z^d. *Z. Wahrscheinlichkeitstheor. Verwandte Geb.* **53**, 183–196 (1980).
26. O. Hallatschek, P. Hersen, S. Ramanathan, D. R. Nelson, Genetic drift at expanding frontiers promotes gene segregation. *Proc. Natl. Acad. Sci. U.S.A.* **104**, 19926–19930 (2007).
27. M. Delarue *et al.*, Self-driven jamming in growing microbial populations. *Nat. Phys.* **12**, 762–766 (2016).
28. D. Bi, X. Yang, M. C. Marchetti, M. L. Manning, Motility-driven glass and jamming transitions in biological tissues. *Phys. Rev. X* **6**, 021011 (2016).
29. A. Giometto, D. R. Nelson, A. W. Murray, Physical interactions reduce the power of natural selection in growing yeast colonies. *Proc. Natl. Acad. Sci. U.S.A.* **115**, 11448–11453 (2018).
30. J. Kayser, C. F. Schreck, M. Gralka, D. Fusco, O. Hallatschek, Collective motion conceals fitness differences in crowded cellular populations. *Nat. Ecol. Evol.* **3**, 125–134 (2018).
31. A. G. O'Donnell, I. M. Young, S. P. Rushton, M. D. Shirley, J. W. Crawford, Visualization, modelling and prediction in soil microbiology. *Nat. Rev. Microbiol.* **5**, 689–699 (2007).
32. K. Z. Coyte, H. Tabuteau, E. A. Gaffney, K. R. Foster, W. M. Durham, Microbial competition in porous environments can select against rapid biofilm growth. *Proc. Natl. Acad. Sci. U.S.A.* **114**, 161–170 (2017).
33. G. Kilbertus *et al.*, Microhabitats in soil aggregates. their relationship with bacterial biomass and the size of the procaryotes present. *Revue d'Ecologie et de Biol. du Sol* **17**, 543–557 (1980).
34. I. Young, K. Ritz, Tillage, habitat space and function of soil microbes. *Soil Tillage Res.* **53**, 201–213 (2000).
35. X. Raynaud, N. Nunan, Spatial ecology of bacteria at the microscale in soil. *PLoS One* **9**, e87217 (2014).
36. D. R. Marshak, R. L. Gardner, D. Gottlieb, *Stem Cell Biology* (Cold Spring Harbor Laboratory Press, 2001).
37. S. M. Janes, S. Lowell, C. Hutter, Epidermal stem cells. *J. Pathol.* **197**, 479–491 (2002).
38. S. P. Bach, A. G. Renehan, C. S. Potten, Stem cells: The intestinal stem cell as a paradigm. *Carcinogenesis* **21**, 469–476 (2000).
39. J. Cairns, Mutation selection and the natural history of cancer. *Nature* **255**, 197–200 (1975).
40. S. A. Frank, *Dynamics of Cancer: Incidence, Inheritance, and Evolution* (Princeton University Press, 2007).
41. M. Vishwakarma, E. Piddini, Outcompeting cancer. *Nat. Rev. Cancer* **20**, 187–198 (2020).
42. A. Di Gregorio, S. Bowling, T. A. Rodriguez, Cell competition and its role in the regulation of cell fitness from development to cancer. *Dev. Cell* **38**, 621–634 (2016).
43. F. Stirling *et al.*, Rational design of evolutionarily stable microbial kill switches. *Mol. Cell* **68**, 686–697 (2017).
44. M. Kaiser *et al.*, Monitoring single-cell gene regulation under dynamically controllable conditions with integrated microfluidics and software. *Nat. Commun.* **9**, 1–16 (2018).
45. L. Saias, J. Autebert, L. Malaquin, J. L. Viovy, Design, modeling and characterization of microfluidic architectures for high flow rate, small footprint microfluidic systems. *Lab Chip* **11**, 822–832 (2011).
46. D. Qin, Y. Xia, G. M. Whitesides, Soft lithography for micro- and nanoscale patterning. *Nat. Protoc.* **5**, 491–502 (2010).
47. C. A. Schneider, W. S. Rasband, K. W. Eliceiri, NIH Image to ImageJ: 25 years of image analysis. *Nat. Methods* **9**, 671–675 (2012).
48. A. Ducret, E. M. Quardokus, Y. V. Brun, MicrobeJ, a tool for high throughput bacterial cell detection and quantitative analysis. *Nat. Microbiol.* **1**, 16077 (2016).